Peer-reviewed version available at *Entropy* **2019**, *21*, 103; doi:10.3390/e21020103

Article

Entropy Generation Optimization for Rarified Nanofluid Flows in a Square Cavity with Two Fins at the Hot Wall

Wael Al-Kouz [1,*], Ahmad Al-Muhtady [2], Wahib Owhaib [2], Sameer Al-Dahidi [2], Montasir Hader [3] and Rama Abu-Alghanam [4]

[1] Mechatronics Engineering Department, German Jordanian University, Amman, 11180, Jordan; wael.alkouz@gju.edu.jo (W. A.); rama.abualghanam@gju.edu.jo (R. A.)
[2] Mechanical and Maintenance Engineering Department, German Jordanian University, Amman, 11180, Jordan; ahmad.almuhtady@gju.edu.jo (A. A.); Wahib.Owhaib@gju.edu.jo (W. O.); Sameer.Aldahidi@gju.edu.jo (S. A.)
[3] Aeronautical Engineering Department, Jordan University of Science and Technology, Irbid, 22110, Jordan; hader@just.edu.jo (M.H.)
[4] Energy Engineering Department, German Jordanian University, Amman, 11180, Jordan; rama.abualghanam@gmail.com (R. A.)

* Correspondence: wael.alkouz@gju.edu.jo; Tel.: +962-6429-4444 (ext. 4519)

Abstract: Computational Fluid Dynamics (CFD) is utilized to study entropy generation for the rarefied steady state laminar 2-D flow of air-Al_2O_3 nanofluid in square cavity equipped with two solid fins at the hot wall. Such flows are of great importance in industrial applications, such cooling of the electronic equipment's and nuclear reactors. In the current study, effects of Knudsen number (Kn), Rayleigh number (Ra) and the nano solid particles volume fraction (ϕ) on the entropy generation are investigated. The values of parameters considered in this work are as follows: $0 \leq Kn \leq 0.1$, $10^3 \leq Ra \leq 10^6$, $0 \leq \phi \leq 0.2$. Length of the fins (L_F) is considered to be fixed and equals to 0.5 m, whereas the location of the fins with respect to the lower wall (H_F) is set to 0.25 and 0.75 m. Simulations demonstrate that there is an inverse direct effect of Kn on the entropy generation. Moreover, it is found that when Ra is less than 10^4, the entropy generation, due to the flow, increases as ϕ increases. In addition, the entropy generation due to the flow will decrease at Ra greater than 10^4 as ϕ increases. Moreover, the entropy generation due to heat will increase as both the ϕ and Ra increase. In addition, a correlation model of the total entropy generation as a function of all of the investigated parameters in this study is proposed. Finally, an optimization technique is adapted to find out the conditions at which the total entropy generation is minimized.

Keywords: natural convection; entropy generation; square cavity; low pressure; nanofluid.

1. Introduction

Cai et al. [1] reported that in recent years, unconventional reservoirs have drawn tremendous attention worldwide; they have discussed a series of recent works on various fractal-based approaches in such reservoirs. They covered many topics including fractal characterization of pore structure and its influence on the physical properties and fluid flow in fracture network under shearing, porous flow phenomena and gas adsorption mechanism. One of the basic problems that is investigated deeply in the last few decades is the natural convection mode of heat transfer that serves in a number of engineering applications, for example solar collectors [2-3], fuel cell industry [4], petroleum engineering [5-6], and cooling of electronic components [7-8], etc. However, the unsatisfying heat-transfer rate due to the natural convection is a significant issue for the application. As a result, dispersion of nano solid particles into a base fluid has been developed as a widely-used method to address such an issue. By dispersing nano solid particles into the base fluid, the resulting

nanofluid will have superior thermal properties compared to the base fluid. For instance, Choi et al. [9] introduced "nanofluids" used in many industrial applications. In the work conducted by Khanafer et al. [10], numerical solution of natural convection heat transfer in two-dimensional enclosure where nanofluid is used as the working fluid is analyzed. They concluded that there is a direct proportional relationship between the heat transfer rate and the ϕ at a given Grashof number. Moreover, Khanafer et.al [11] studied the validity of nanofluids effective viscosity and thermal conductivity models along with experimental results available in the literature and their features in enhancement of heat transfer. Buongiorno [12] discussed and provided explanation to the convective heat transfer enhancement associated with using nanofluid. He proposed a new model for transport phenomena in nanofluids based on two-component nonhomogeneous equilibrium model. In Oztop et al. [13], CFD analysis is used to solve a mathematical model for fluid flow and heat transfer due to buoyancy effect in a partially heated cavity filled with nanofluid. They noticed that at a given *Ra*, there is an enhancement in heat transfer as ϕ increases. In addition, Ghasemi et al. [14] numerically studied the natural convection of water/Al_2O_3 nanofluid in square cavity under a magnetic field. They found that for any ϕ, heat transfer rate is strongly dependent on *Ra*; it may enhance or deteriorate. Also, Kefayati et al. [15] simulated the heat transfer and flow of free convection in cavities filled with water/SiO_2 using lattice Boltzmann method. They concluded that there is a direct relationship between the heat transfer rate and ϕ for the studied aspect ratios and *Ra*. Additionally, Kefayati [16] analyzed entropy generation and heat transfer of laminar free convection flow in porous square cavity filled with non-Newtonian nanofluid Cu/water using finite difference lattice Boltzmann method. He found that the heat transfer rate is enhanced and entropy generation is dropped when both ϕ and *Ra* are increased. Al-Kouz et al. [17] numerically investigated free convection heat transfer characteristics of rarefied flows in an inclined square enclosure equipped with two solid or porous fins at the hot wall. They found that with equipped fins to the hot wall, the heat transfer rate is enhanced. Moreover, they found that using porous fins has advanced impact on heat transfer. Al-Kouz et al. [18] numerically studied low-pressure gaseous flows free convection heat transfer characteristics of nanofluid (Air-Al_2O_3) inside a square enclosure equipped with two solid fins at the hot wall. They revealed that for a given *Ra*, adding nanoparticles results in enhancement in heat transfer rate.

Studying the rate of entropy generation is important in engineering because it suitably calculates thermodynamics irreversibilties. For example, Kefayati et al. [19] analyzed the natural convection flow in inclined cavity of non-Newtonian nanofluid using Buongiorno's mathematical model by finite difference lattice Boltzmann method. They observed that the lowest entropy generation and highest Bejan number occur at inclined angle of zero at given *Ra*. Parvin et al. [20] numerically investigated entropy generation and laminar free convective heat transfer in an odd-shaped enclosure filled with Cu-water nanofluid. Their results revealed that with increasing *Ra*, entropy generation caused by heat is increased while the entropy generation caused by the fluid flow is decreased. They also extracted the optimum value of *Ra* at which the heat transfer is maximized and the total entropy generation is minimized. In the work of Merji et al. [21] and Mahmoudi et al. [22], numerical study using Lattice Boltzmann method for the laminar free convection and entropy generation in a square enclosure filled with water/Al_2O_3 nanofluid under a magnetic field is conducted. They found that ϕ has a direct effect on the heat transfer rate and an inverse effect on the total entropy generation. In the article by Armaghani et al. [23], a numerical study of the entropy generation and natural convection heat transfer in baffled L-shaped cavity filled with water-Alumina nanofluid has been presented. The authors revealed that as the aspect ratio increases, the heat transfer rate enhances particularly when nanofluid is utilized as a working fluid. Al-Zamily [24] numerically studied the influence of porous central layer thickness inside a cavity on heat transfer, fluid flow and entropy generation. The cavity is filled with nanofluid (water/ TiO_2) at constant wall heat flux located at two different wall positions. Results show that the nanofluid flow is stronger and heat transfer rate increases as the central porous layer thickness decreases. He also concluded that the heat transfer rate is enhanced with ϕ. Bouchouch et al. [25] investigated the free convection heat transfer and entropy generation of nanofluid (water/ Al_2O_3) in a square enclosure with thick bottom wall heated with non-isothermal heater with sinusoidal function. The authors have shown that using the nanofluid enhances the heat transfer. Moreover, they concluded that the entropy generation increases with *Ra*.

Ashorynejad et al. [26] numerically investigated entropy generation of free convection heat transfer in a square porous enclosure with various porosities filled with different water base nanofluids (Al_2O_3, TiO_2 and CuO) using Lattice Boltzmann method. They concluded that dispersion of nano solid particles decreases the total entropy generation and enhances heat transfer. They also concluded that the entropy generation is increased with cavity porosity. In their work, Sheremet et al. [27] studied numerically free convection heat transfer and entropy generation of water based nanofluid inside square cavity with variable temperature distribution sidewalls. They concluded that the total entropy generation increases with *Ra* and rise of the temperature distribution sidewalls amplitude. Alsabery et al. [28] numerically investigated free convection and entropy generation of nanofluid (water/ Al_2O_3) in square enclosure with a concentric solid inserts and different temperature distributions. They observed a strong heat transfer rate enhancement with increasing *Ra* for a given Rayleigh number range. In addition, they concluded that the total entropy generation rises with increasing *Ra* and reduction in the size of the concentric solid insert beyond a given *Ra*. A numerical investigation using the two-phase mixture and Darcy-Birnkman-Forchheimer model for the free convection, and entropy generation of nanofluid (water / Cu) inside a cavity furnished with porous fins is presented by Siavashi et al. [29]. They revealed that low ϕ enhances the heat transfer rate at a given *Ra*. They also found that the thermal irreversibility is dominant pertaining to friction entropy generation. Finally, they concluded that the entropy generation is reduced by using porous fins. Kashyap et al. [30] numerically investigated using two-phase lattice Boltzmann the natural convection of nanofluid (water/Cu) in porous square cavity at different boundary conditions. They observed that for all the boundary conditions they studied, the use of nanofluid enhances the heat transfer and reduces the entropy generation depending on ϕ. Gibanov et al. [31] analyzed numerically the free convection heat transfer and entropy generation of nanofluid (water-Alumina) in a lid-driven cavity with a bottom solid wall. They concluded that ϕ has a direct effect on the heat transfer. Mansour et al. [32] numerically investigated the entropy generation and magneto-hydrodynamics (MHD) natural convection heat transfer in a square porous enclosure filled with hybrid nanofluid (water-Cu-Al_2O_3). They revealed that for a given *Ra*, the heat transfer rate is decreased and entropy generation is increased with increasing ϕ. Rahimi et al. [33] investigated natural convection heat transfer and entropy generation of nanofluid (water-CuO) inside a square cavity equipped with fins. They concluded that heat transfer rate increases with increasing *Ra* and ϕ, whereas entropy generation increases with *Ra* and decreases with ϕ for the investigated parameters ranges. In their paper, Rashidi et al. [34] investigated the effects of different modeling approaches on the entropy generation in circular tube heat exchanger using nanofluids, the considered geometry is a horizontal tube with constant wall heat flux. The flow regime is turbulent. They found out that the values for entropy generation are very close for the single phase and mixture models. Additionally, they concluded that for higher volume fractions (i.e. greater than 4%), differences between the models appear. In their work, Yarmand et al. [35], studied numerically entropy generation during turbulent flow of Zirconia-water and other nanofluids in square cross section tube with a constant heat flux, the flow is assumed to be turbulent. Their results show that the optimal volume concentration of nanoparticles to minimize the entropy generation increases when Reynolds number decreases, it was also found that the thermal entropy generation increases with the increase of nanoparticle size whereas the frictional entropy generation decreases. Entropy generation in thermal radiative loading of structures with distinct heaters have been studied numerically by Jamalabadi et al. [36], they used finite volume analysis and the semi implicit method for pressure linked equations to solve for the continuity, momentum and energy equations, their results show that the entropy value was most influenced by temperature than the density. They also showed that the heating ratio of onset of natural and radiative entropy generation increases by an increase of number of discrete heater sources. In their research, Aghaei et al. [37] analyzed experimentally and numerically the effect of horizontal and vertical elliptic baffles inside an enclosure on the mixed convection of a MWCNTs-water nanofluid and its entropy generation, they concluded that horizontal placement of thermal baffle led to a higher heat transfer rate. Moreover, they found that the entropy generation values in the horizontal position were higher than the vertical position. Mahmoudinezhad et al. [38] investigated numerically and experimentally the adiabatic partition effect on natural convection heat transfer inside a square

cavity, the flow is considered to be steady state, 2-D. They used finite volume analysis along with Mach-Zehender interferometer to carry out the study. Their results show that that average Nusselt number increases by increasing Rayleigh number. However, for a given *Ra*, the maximum and minimum heat transfer occurs at partition angles of 45° and 90°, respectively. Finally, Nasiri et al. [39] used a smoothed particle hydrodynamics approach to investigate forced convection nanofluid heat transfer over a horizontal cylinder. Their results show that the smoothed particle hydrodynamics approach is appropriate method for such numerical modeling. In addition, they concluded that nanofluid heat transfer characteristics marked improvements compared to base fluids.

Despite many studies in the field of entropy generation deal with water-based nanofluid inside square cavities, there is lack in studies that tackle the entropy generation of natural convection low-pressure cavities filled with air based nanofluid. Therefore, the purpose of the present numerical investigation is to give more insight into the entropy generation in square cavities equipped with two solid fins at the hot wall filled with low-pressure air/Al_2O_3 nanofluid. Analyzed parameters include Rayleigh number ($10^3 \le Ra \le 10^6$) to cover both conduction dominant and convection dominant modes of heat transfer, Knudsen number ($0 \le Kn \le 0.1$) to cover both slip and continuum flow regimes, and nanosolid particles volume fraction ($0 \le \phi \le 0.2$).

2. Mathematical Modeling

2.1 Mathematical Formulation

In this study, two dimensional steady state laminar natural convection of air-Al_2O_3 nanofluid flow is investigated. Due to a small temperature difference between the hot and cold walls, all of the thermophysical properties of the nanofluid are assumed constant except for the density variation that is modeled using the Boussinesq approximation. Figure 1 represents the geometry characterized as a square cavity of length *L* with two fins at the hot wall in the study. In this study, both slip and continuum flow regimes are analyzed.

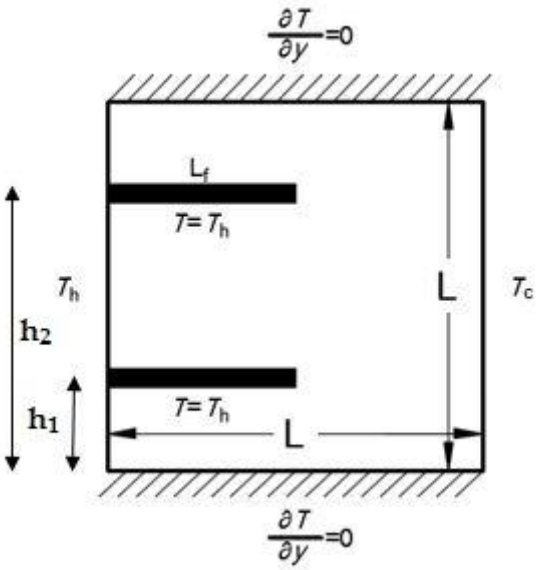

Figure 1. The configuration used for the computational domain $\mathbf{h_1}$

Dispersing nanoparticles to the base fluid will enhance the thermophysical properties of the resulting nanofluid. Reported in Al-Kouz et al. [10], these properties can be calculated based on the following equations:

Viscosity:

$$\mu_{nf} = \frac{\mu_f}{(1 - \emptyset)^{2.5}} \tag{1}$$

Density:

$$\rho_{nf} = (1 - \emptyset)\rho_f + \emptyset\rho_s \tag{2}$$

Heat Capacitance:

$$C_{P_{nf}} = (1 - \emptyset)(C_P)_f + \emptyset(C_P)_s \tag{3}$$

Thermal Expansion Coefficient:

$$\beta_{nf} = \beta_f \left[\frac{1}{1 + \frac{(1 - \emptyset)\rho_f}{\emptyset\rho_s}\frac{\beta_s}{\beta_f}} + \frac{1}{1 + \frac{\emptyset}{1 - \emptyset}\frac{\rho_s}{\rho_f}} \right] \tag{4}$$

Thermal Conductivity:

$$k_{nf} = k_f \frac{k_s + 2k_f - 2\emptyset(k_f - k_s)}{k_s + 2k_f + \emptyset(k_f - k_s)} \tag{5}$$

Table 1 shows the thermophysical properties utilized to obtain the resulting properties of the Al_2O_3-air nanofluid.

Table 1. Thermophysical properties of air and Al_2O_3.

Physical Properties	Air	Al_2O_3
Cp (J/kg K)	1006.43	765
ρ [kg/m^3]	1	3970
k [W/m^{2}K]	0.025	40
β [1/K]	0.00333	0.0000085
α [m^2/s]	0.000019	0.00001317

The governing equations of the current study are reported in Al-Kouz et al. [18] and are summarized below:

Continuity:

$$\frac{\partial u}{\partial x} + \frac{\partial v}{\partial y} = 0 \tag{6}$$

x- momentum:

$$\rho_{nf}\left(u\frac{\partial u}{\partial x} + v\frac{\partial u}{\partial y}\right) = -\frac{\partial P}{\partial x} + \mu\left[\frac{\partial^2 u}{\partial x^2} + \frac{\partial^2 u}{\partial y^2}\right] \tag{7}$$

y-momentum:

$$\rho_{nf}\left(u\frac{\partial v}{\partial x}+v\frac{\partial v}{\partial y}\right)=-\frac{\partial P}{\partial y}-\rho_{nf}g+\mu[\frac{\partial^2 v}{\partial x^2}+\frac{\partial^2 v}{\partial y^2}] \quad (8)$$

Energy:

$$\rho_{nf}C_{p_{nf}}\left(u\frac{\partial T}{\partial x}+v\frac{\partial T}{\partial y}\right)=k_{nf}[\frac{\partial^2 T}{\partial x^2}+\frac{\partial^2 T}{\partial y^2}] \quad (9)$$

With the following boundary conditions in the slip flow regime as reported in Karniadakis et al. [40], Lockerby et al. [41] and Colin [42]:

$$u_w-u_g=\left(\frac{2-\sigma_v}{\sigma_v}\right)\lambda\frac{\partial u}{\partial n}\approx\left(\frac{2-\sigma_v}{\sigma_v}\right)K_n(u_g-u_c) \quad (10)$$

$$v_g=0 \quad (11)$$

$$T_w-T_g=\left(\frac{2-\sigma_T}{\sigma_T}\right)\frac{2\gamma}{\gamma+1}\frac{k}{\mu c_v}\lambda\frac{\partial T}{\partial n}\approx\left(\frac{2-\sigma_T}{\sigma_T}\right)\frac{2\gamma}{\gamma+1}\frac{k}{\mu c_v}(T_g-T_c) \quad (12)$$

In equations 10 and 12, σ_v and σ_T refer to the momentum and thermal accommodation coefficients, respectively, and Kn is defined as:

$$K_n=\frac{\lambda}{L} \quad (13)$$

where L is the square cavity characteristic length and λ is the mean free path.

The imposed thermal boundary conditions at x= 0 and L:

$$At(x=0,y),T=T_h \quad (14)$$

$$At(x=L,y),T=T_c \quad (15)$$

where T_h is the temperature at the hot surface and T_c is the temperature at the cold surface, the fins temperature is set to T_h

In order to calculate the local heat fluxes, and referring to Al-Kouz et al. [18],equations 16 and 17 are utilized:

$$q_F''=-k\frac{\partial T}{\partial n}|_F \quad (16)$$

$$q_h''=-k\frac{\partial T}{\partial n}|_h, q_c''=-k\frac{\partial T}{\partial n}|_c \quad (17)$$

To calculate the total heat transfer from the hot to the cold wall , one should integrate the local heat flux along the wall of the hot wall combined with the fins as follows:

$$Q = \sum \left(\int_{A_h} q_h'' \, dA_h + \int_{A_F} q_F'' \, dA_F \right) = \int_{A_c} q_c'' \, dA_c \tag{18}$$

Then, the average heat transfer coefficient along combined hot wall and the fins or along the cold surface is derived as follows:

$$\bar{h} = \frac{Q}{(T_i - T_o)A_T} = \frac{Q}{(T_i - T_o)A_c} \tag{19}$$

From the previous equation, one can derive the average Nusselt number for L= 1m, where:

$$Nu = \frac{\bar{h}L}{k_{n_f}} = \frac{\bar{h}}{k_{nf}} \tag{20}$$

Following Parvin et al. [20], the total entropy generation is defined as:

$$Sgen_{tot} = Sgen_f + Sgen_h \tag{21}$$

In equation 21, $Sgen_f$ is the entropy generation caused by the flow and $Sgen_h$ is the entropy generation due to heat

where,

$$Sgen_f = \frac{k_{nf}}{{T_o}^2} \left[\left(\frac{\partial T}{\partial x} \right)^2 + \left(\frac{\partial T}{\partial y} \right)^2 \right] \tag{22}$$

$$Sgen_h = \frac{\mu_{nf}}{T_o} \left[2 \left(\frac{\partial u}{\partial x} \right)^2 + 2 \left(\frac{\partial v}{\partial y} \right)^2 + \left(\frac{\partial u}{\partial x} + \frac{\partial v}{\partial y} \right) \right] \text{ and } T_o = \frac{T_h + T_c}{2} \tag{23}$$

2.2 Numerical Solution

In this study, a finite volume technique is utilized using ANSYS Fluent software to investigate flow, heat transfer characteristics and the total entropy generation for steady, 2D, laminar natural convection rarefied nanofluid in square cavity. The SIMPLE algorithm presented by Versteeg and Malalasekera [43] and Patankar and Spalding [44] is utilized. In order to calculate the pressure field, PRESTO algorithm is used. Moreover, a hybrid second order accuracy scheme of upwind and central difference is used to differentiate the convective terms. As a starting point, a 40×40 mesh elements are tested. In addition, σ_v and σ_T for all simulations are considered to be unity. The solution is converged when the maximum of the normalized absolute residual across all nodes is $< 10^{-6}$.

2.3 Grid Independency

The grid that is used in all simulations is a two dimensional mesh and it is shown in Figure 2. Initially, the step sizes of the grid are increasing in the x and y directions with expansion factors of 1.06 and 1.15 respectively, these values were selected to capture the gradients near solid-fluid interface. Then the mesh was adapted in which velocity gradients near the solid surfaces are calculated. After this, the number of cells is increased to lower the gradients below a certain value. It was noticed that any further change in these parameters would not affect the results. A grid independency test is performed by monitoring Nu at the cold surface, and solutions for different numbers of grid nodes were obtained. It was obvious that adding more cells beyond a certain value will not affect Nu. In addition, the average magnitude of the velocity inside the cavity was monitored

Preprints (www.preprints.org) | NOT PEER-REVIEWED | Posted: 8 January 2019 doi:10.20944/preprints201901.0074.v1

Peer-reviewed version available at Entropy 2019, 21, 103; doi:10.3390/e21020103

and tabulated. Table 2. summarizes the values of Nu as well the velocity magnitude inside the cavity along with their relative error to the values obtained for mesh size of 100x100 elements

Figure 2. 2D mesh utilized in all simulations.

Figure 3 and table.2 demonstrate that the solution is converged for a 100×100 nodes grid size. This grid size is considered for all simulations conducted in this study.

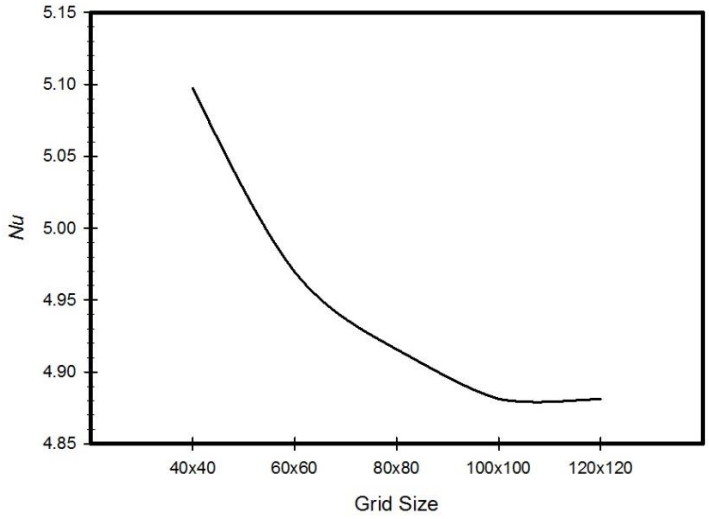

Figure 3. Grid independency test for Nusselt number.

Table 1. Mesh independency test.

Mesh size	Average velocity [m/s]	Relative error in the average velocity %	*Nu*	Relative error in *Nu* %	Simulation time [s]
40x40	0.00055464421	0.050516	5.0973	0.044250507	415
60x60	0.00057143194	0.021778	4.9694	0.01804847	622
80x80	0.00057617336	0.013661	4.9157	0.00704730	739
100x100	0.00058415352	0.0	4.8813	0.0	823
120x120	0.00058415352	0.0	4.881297	6.15e-7	876

2.4 Code Verification

Preprints (www.preprints.org) | NOT PEER-REVIEWED | Posted: 8 January 2019 doi:10.20944/preprints201901.0074.v1

Peer-reviewed version available at Entropy 2019, 21, 103; doi:10.3390/e21020103

For verification purposes, results of the current code are compared with the results extracted by Parvin et al. [12] for the case of an odd shape enclosure filled with Cu-water nanofluid. Figure 4 shows a comparison between the entropy generation caused by the flow and entropy generation due to heat obtained by the current code and those obtained by Parvin et al. [12] at ϕ= 5%, comparisons show satisfactory agreement with an error of less than 1%.

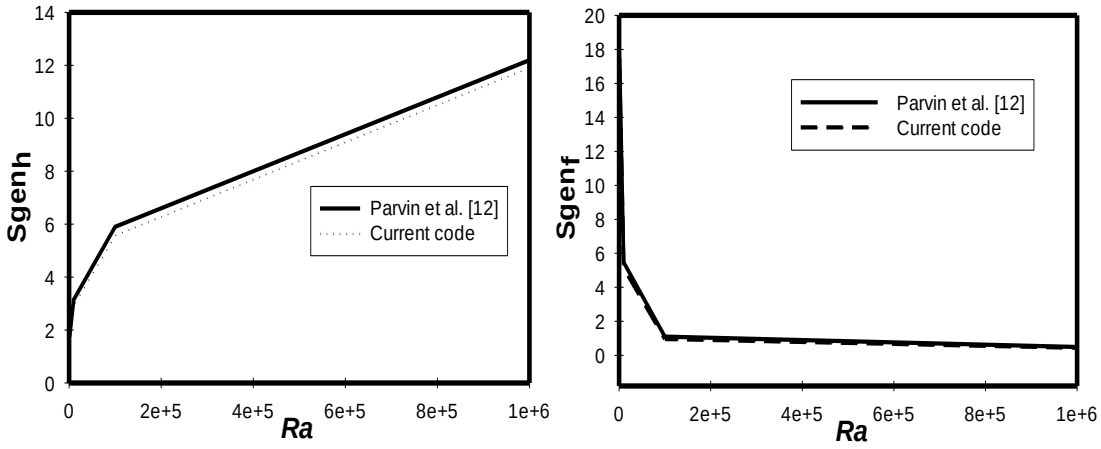

Figure 4. Validation of the current code.

3. Results and discussion

Figures 5, 6 and 7 show the total entropy generation contours inside the square cavities with a fin position of H_F= 0.25, 0.75 m and fin lengths of 0.5 m for the cases where Kn= zero, 0.05 and 0.1 to cover both of the slip and continuum flow regimes. Moreover, ϕ = 0, 0.01, 0.1 and 0.2 are considered. The contours are plotted for cases where Ra=10^3, 10^4 and 10^5. It is clear from the contours that there is a formation of a large clockwise rotating cell. By increasing Kn for the same ϕ and Ra, less circulation is observed inside the cavity. This decrease will affect the heat transfer characteristics. For the cases of ϕ= 0.2 and different Kn, more distortion to the flow is observed compared to the other values of ϕ. The more recirculation and distorted contours will lead to better heat transfer enhancement. Moreover, figures show that as Ra increases for the same Kn and ϕ, more distortion of the contours will occur inside the cavity, so entropy generation will increase due to the increase in the velocity gradients. But still the entropy generation caused by heat is dominant.

Preprints (www.preprints.org) | NOT PEER-REVIEWED | Posted: 8 January 2019 doi:10.20944/preprints201901.0074.v1

Peer-reviewed version available at Entropy 2019, 21, 103; doi:10.3390/e21020103

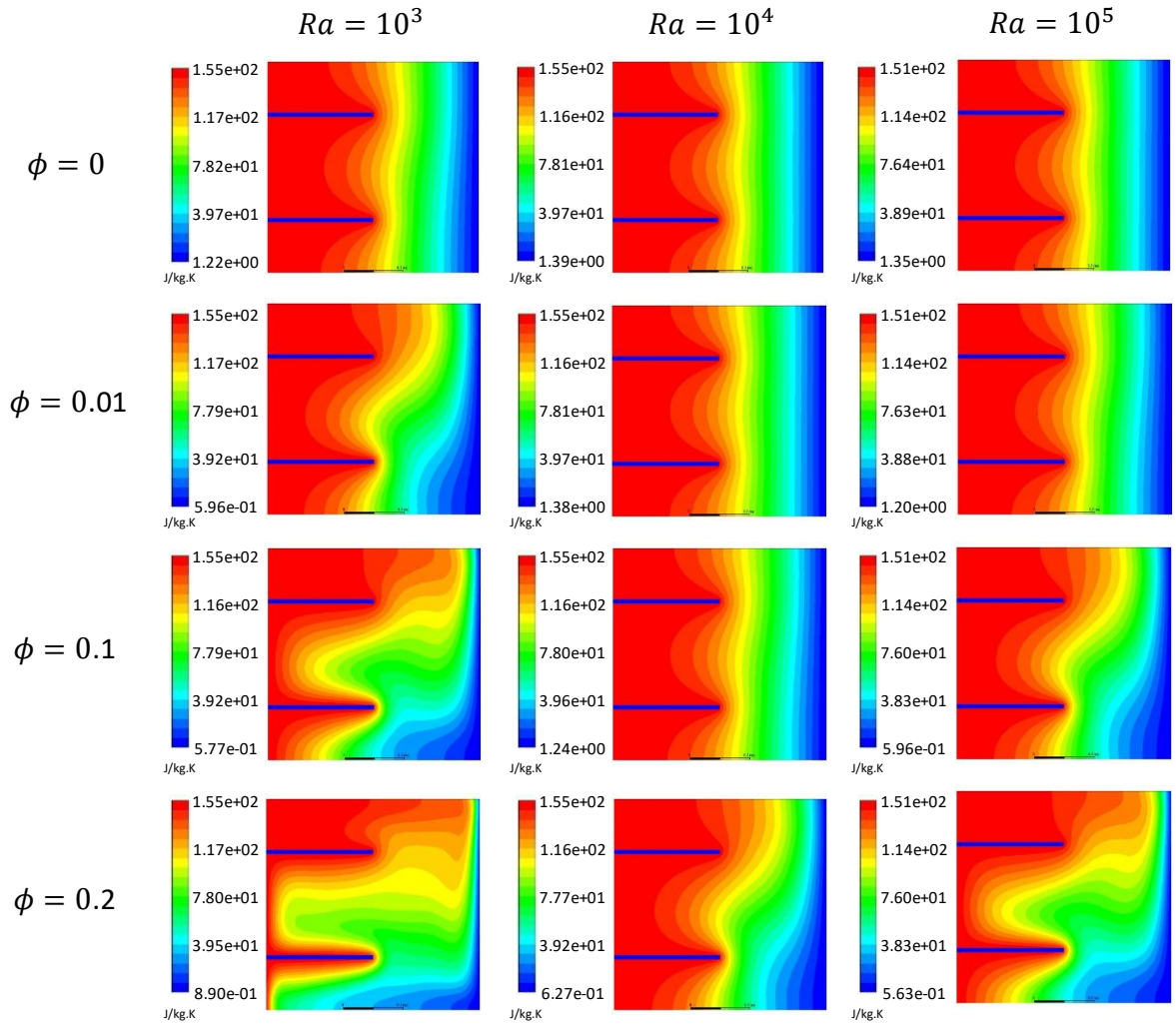

Figure 5. Total entropy generation contours, *Kn*=0 at at different nanoparticles volume fractions (ϕ = 0, 0.01, 0.1 and 0.2) and *Ra*=10^3, 10^4 and 10^5.

Preprints (www.preprints.org) | NOT PEER-REVIEWED | Posted: 8 January 2019 doi:10.20944/preprints201901.0074.v1

Peer-reviewed version available at Entropy 2019, 21, 103; doi:10.3390/e21020103

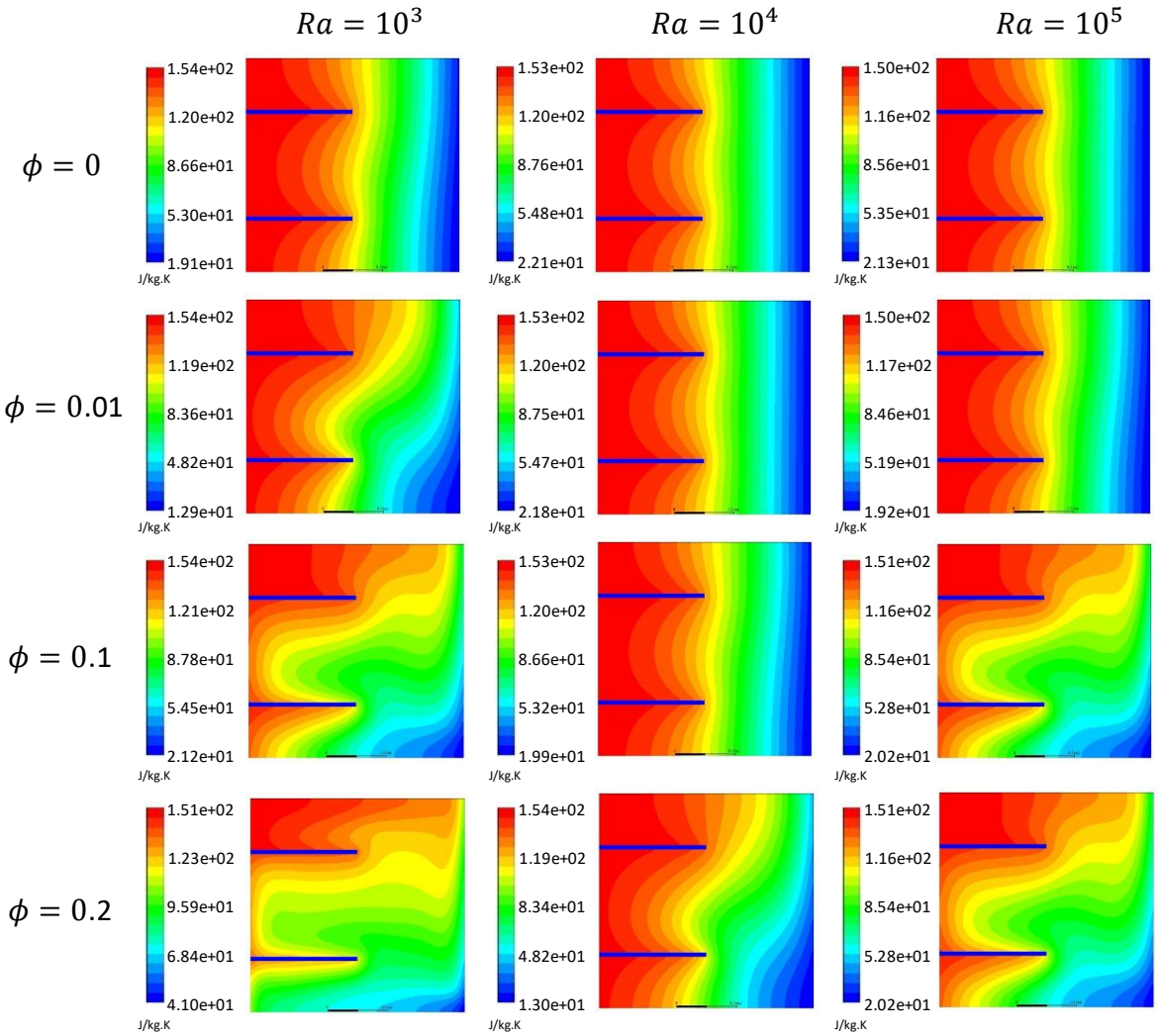

Figure 6. Total entropy generation contours, Kn=0.05 at different nanoparticles volume fractions (ϕ = 0, 0.01, 0.1 and 0.2) and Ra=10^3, 10^4 and 10^5.

Preprints (www.preprints.org) | NOT PEER-REVIEWED | Posted: 8 January 2019 doi:10.20944/preprints201901.0074.v1

Peer-reviewed version available at Entropy 2019, 21, 103; doi:10.3390/e21020103

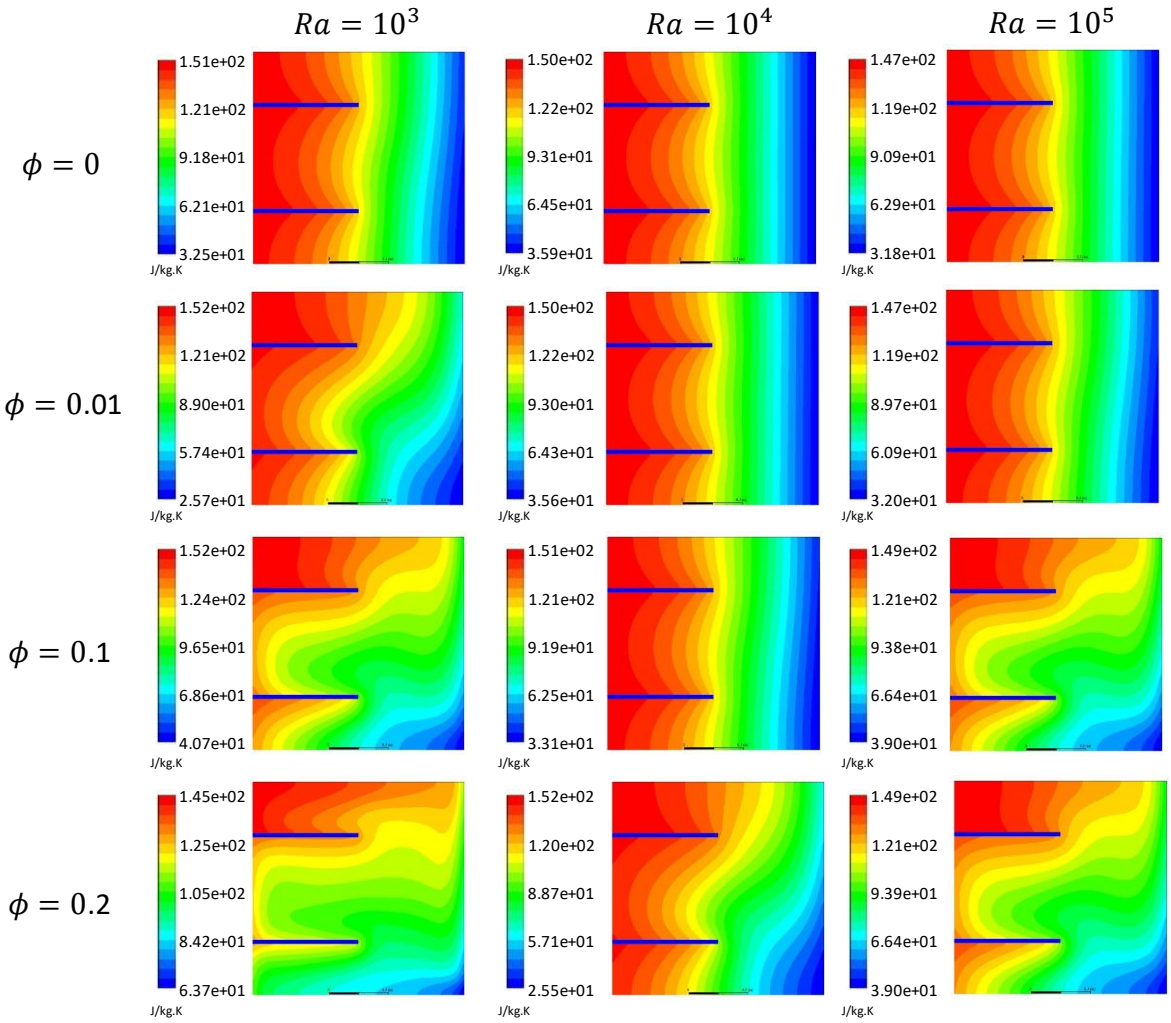

Figure 7. Total entropy generation contours, *Kn*=0.1 at different nanoparticles volume fractions (ϕ= 0, 0.01, 0.1 and 0.2) and *Ra*=10^3, 10^4 and 10^5.

Figure 8 illustrates variations of the entropy generation caused by heat with the nano solid particles volume fraction at different *Kn* for the cases of *Ra*=1000 and 10000. The graphs show that for the two values of *Ra*, as the ϕ increases then the entropy generation due to heat increases as well. This can be attributed to the fact that at low *Ra*, the dominant mode of heat transfer is conduction; by adding nano solid particles, k_{eff} will increase and a better heat transfer is achieved. Better heat transfer implies increase in the entropy generation due to heat. Moreover, the graphs show that as *Kn* increases for the same ϕ then the entropy generation due to heat will decrease. Higher *Kn* will result in more rarefaction effects and consequently less interaction between the nanofluid particles; this will lead to less entropy generation. Finally, the graphs also show that for the higher *Ra*, the entropy generation due to heat will increase for the same value of *Kn* and nano solid particles volume fraction. In figures 5-8, as Ra increases, convection becomes the dominant mode of heat transfer, so more circulation of the flow happens and consequently an increase in the total entropy generation is observed.

Preprints (www.preprints.org) | NOT PEER-REVIEWED | Posted: 8 January 2019 doi:10.20944/preprints201901.0074.v1

Peer-reviewed version available at Entropy 2019, 21, 103; doi:10.3390/e21020103

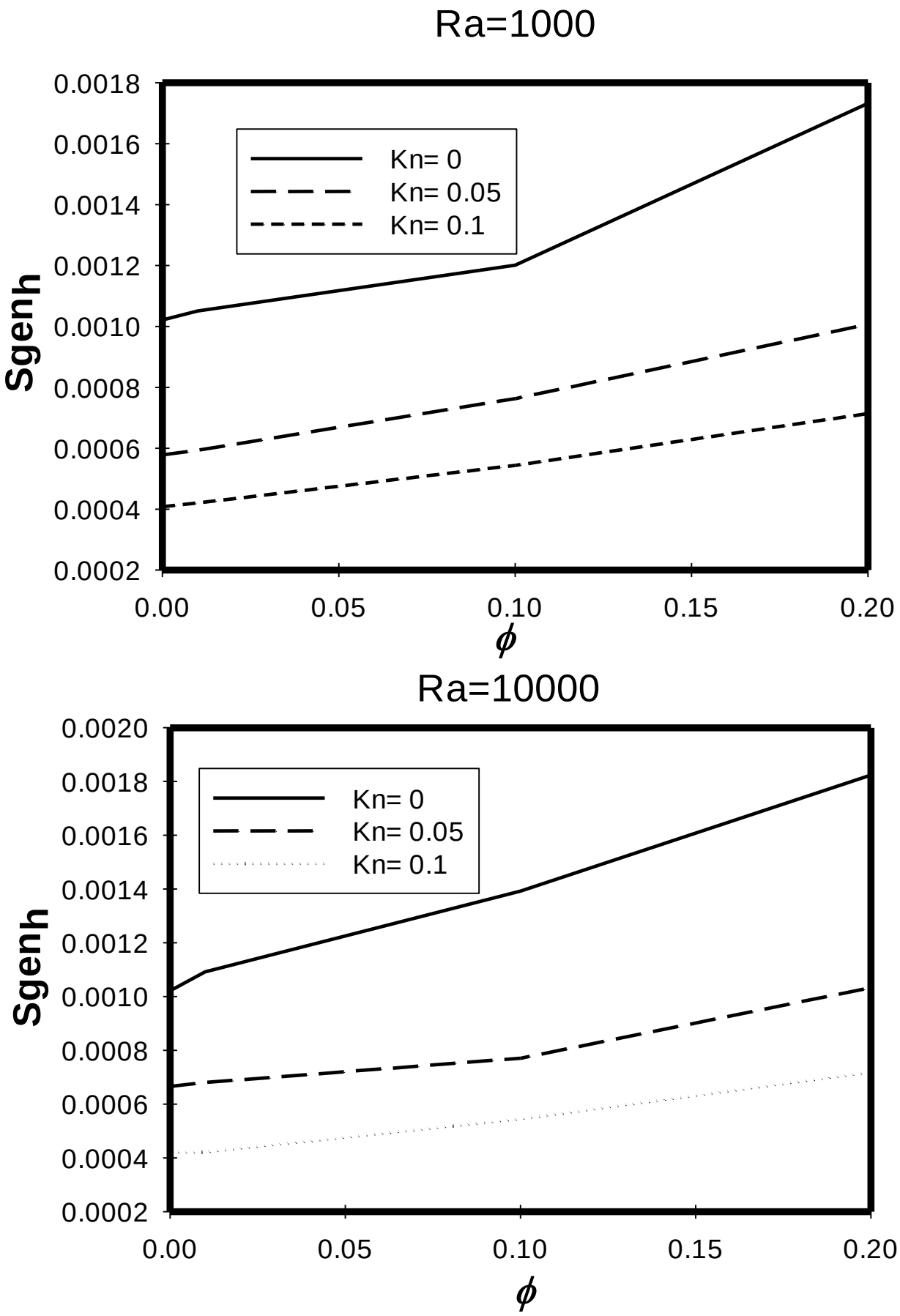

Figure 8. Variation of $Sgen_h$ with ϕ at different *Kn*, *Ra*= 1000, 10000.

Preprints (www.preprints.org) | NOT PEER-REVIEWED | Posted: 8 January 2019 doi:10.20944/preprints201901.0074.v1

Peer-reviewed version available at Entropy 2019, 21, 103; doi:10.3390/e21020103

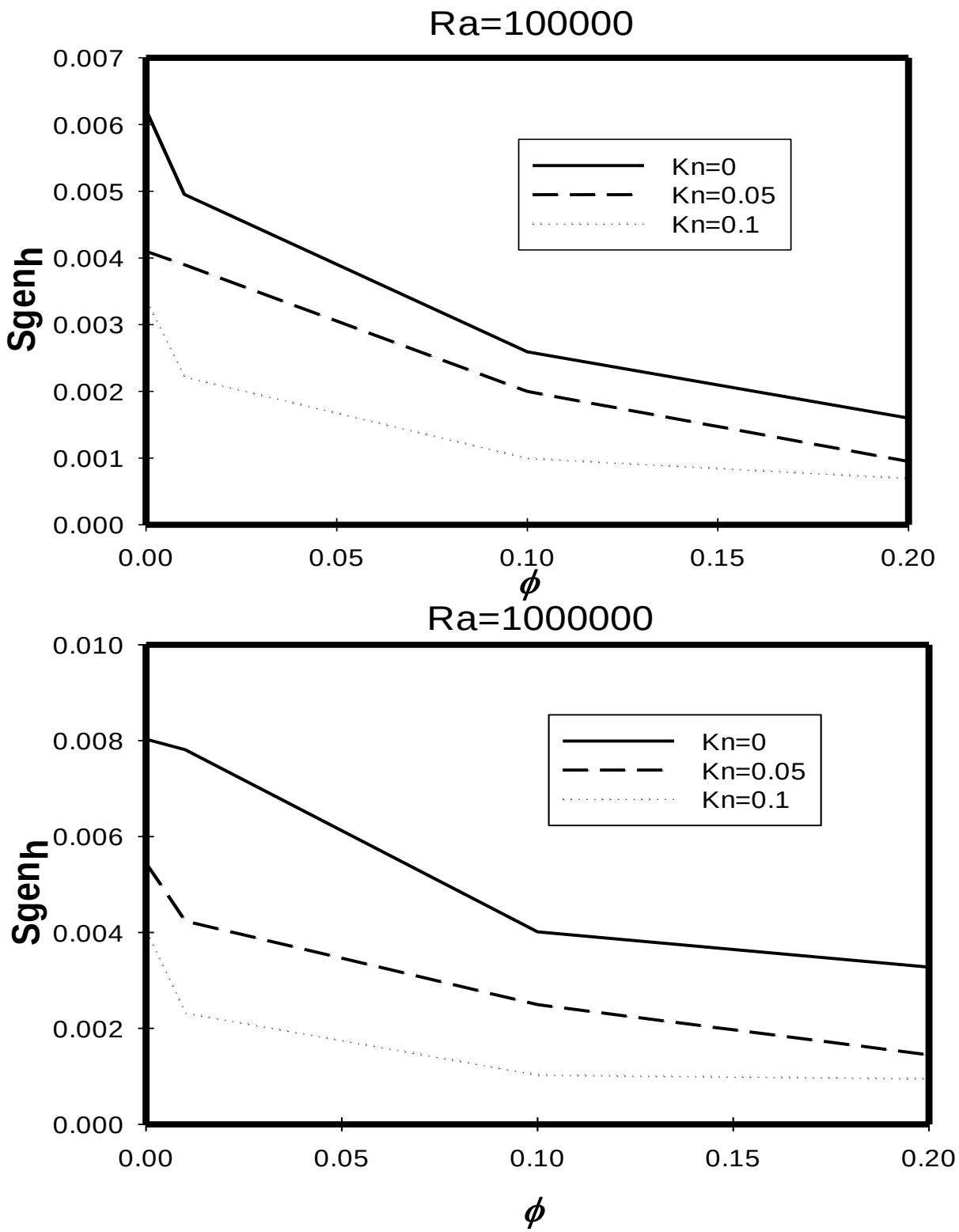

Figure 9. Variation of $Sgen_h$ with ϕ at different *Kn*, *Ra*= 100000, 1000000.

Figure 9 shows variations of the entropy generation due to heat with the nano solid particles volume fraction at different *Kn* for the cases of $Ra=10^5$ and 10^6. The graphs show that for the two values of *Ra*, as the ϕ increases then the entropy generation due to heat decreases. This is mainly due to the fact that at high *Ra*, the dominant mode of heat transfer is convection; by adding nano solid particles, lowering effect of nano solid particles on convection heat transfer becomes dominant. Moreover, graphs show that higher *Kn* will result in less entropy generation. Finally, the graphs also

show that for the higher *Ra*, the entropy generation due to heat will increase for the same value of *Kn* and ϕ.

Variations of the entropy generation due to the flow with *Ra* at different values of nano solid particles volume fractions are plotted in figure 10. The graph shows that as *Ra* increases, then the entropy generation due to the flow will increase. As *Ra* increases, more circulation occurs inside the cavity, so velocity gradient and entropy generation increases. Moreover, as *Kn* increases, the entropy generation due to flow will decrease; this is mainly due to the rarefaction effects. Finally, as the nano solid particles volume fraction increases, then the entropy generation will increase due to the flow (friction) effects.

Preprints (www.preprints.org) | NOT PEER-REVIEWED | Posted: 8 January 2019 doi:10.20944/preprints201901.0074.v1

Peer-reviewed version available at Entropy 2019, 21, 103; doi:10.3390/e21020103

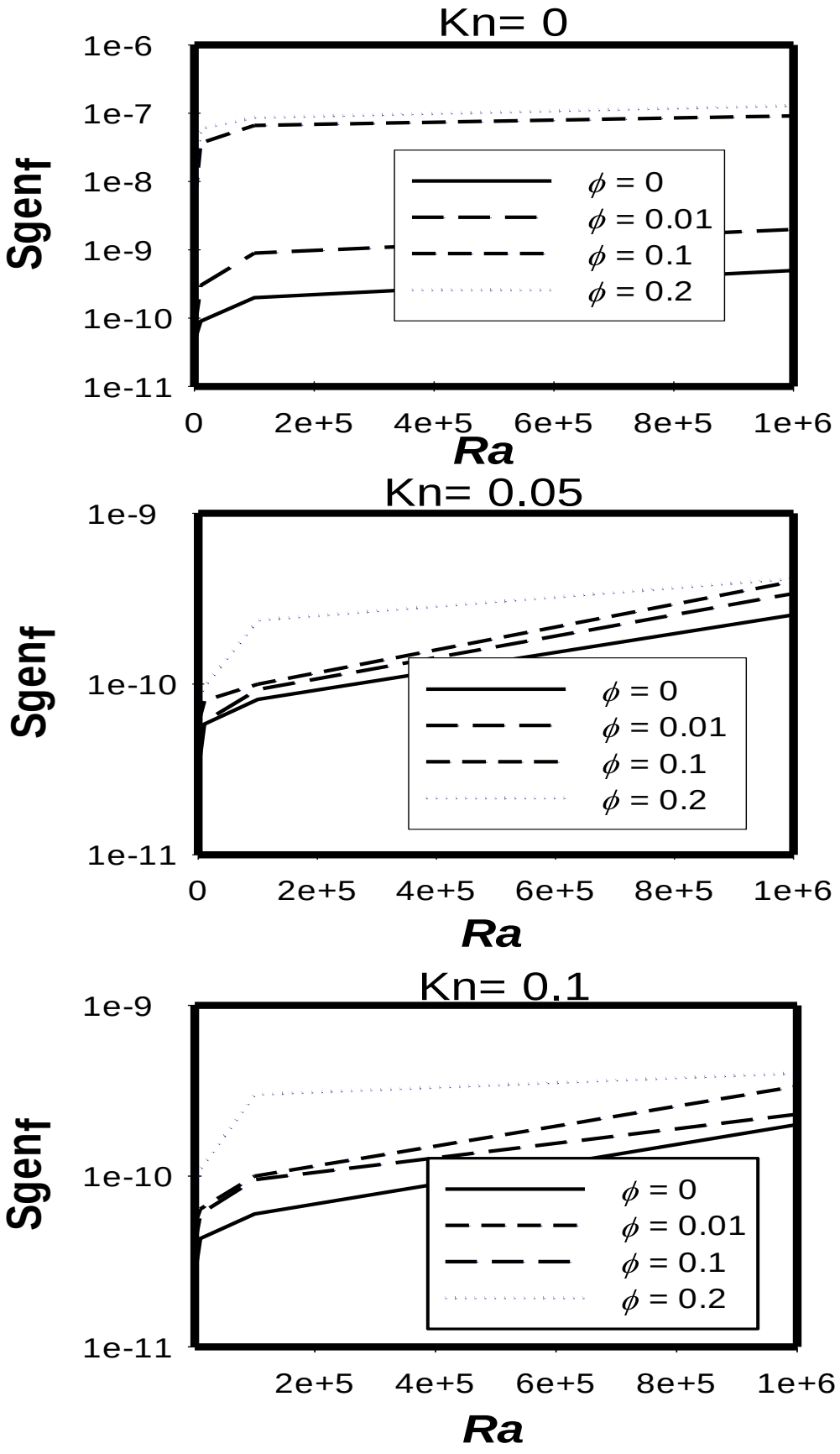

Figure 10. Variation of $Sgen_f$ with Ra at different ϕ, Kn= 0, 0.05 and 0.1.

Preprints (www.preprints.org) | NOT PEER-REVIEWED | Posted: 8 January 2019 doi:10.20944/preprints201901.0074.v1

Peer-reviewed version available at Entropy 2019, 21, 103; doi:10.3390/e21020103

Based on the simulation results, a correlation of the entropy generation among all parameters considered in this study with R^2=0.92 is presented as follows:

$$S_{gen,tot} = C_1 C_2^{Kn} Ra^{C_3} C_4^{\phi} \quad (24)$$

Where, C_1= 2.2e-4 kJ/kg.K, C_2= 0.134, C_3= 0.226, C_4= 0.0077

It is obvious that Bejan number is close to unity for all simulations conducted in the study. Bejan number (*Be*) is defined as follows:

$$Be = \frac{Sgen_h}{Sgen_{tot}} \quad (25)$$

Figure 11 shows a comparison between the total entropy generation results obtained from the simulations with those obtained from the correlations, the figure shows that there is a great match between the simulation and the correlation results. Deviations between the two are noticed for the conditions at which Kn= 0 and ϕ= 0.

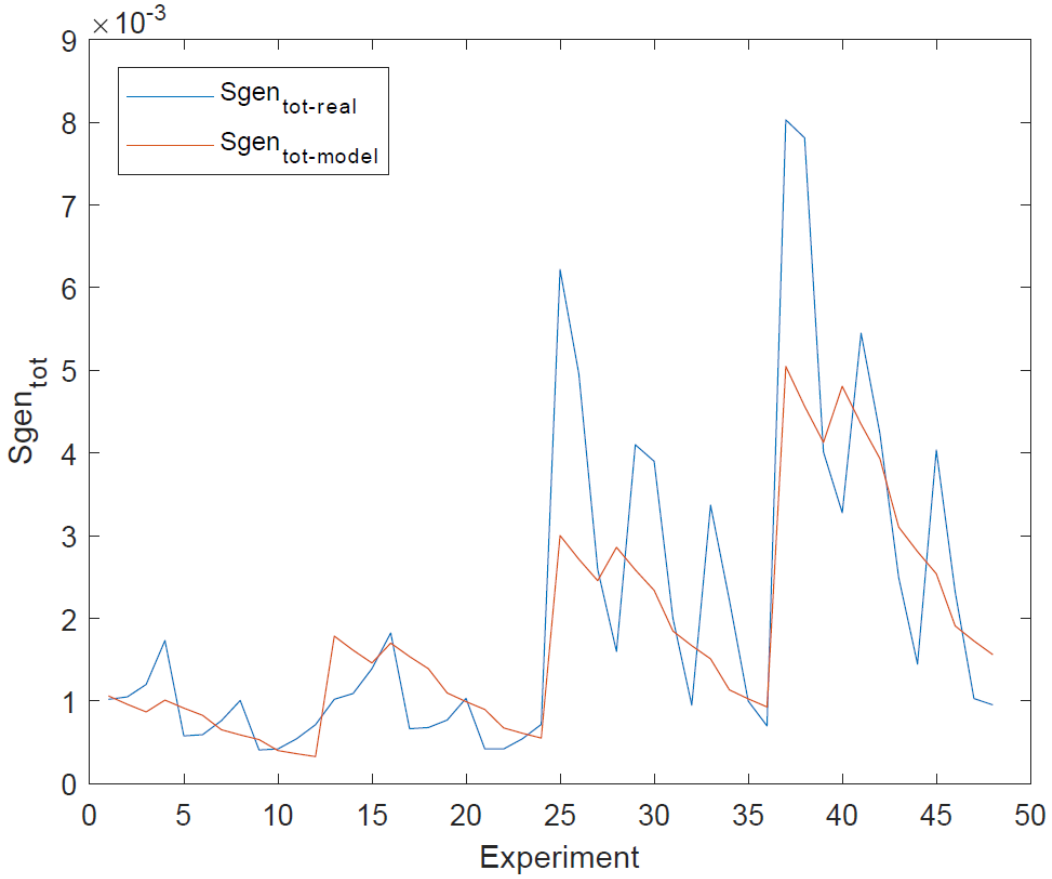

Figure 11. Comparison between the $Sgen_{tot}$ obtained by simulations and those obtained by correlations.

Using Minitab software, design of experiments for the simulations conducted in this work is shown in Figures (12, 13, 14 and 15). Figure 12 shows the main effects of (*Kn*, *Ra* and ϕ) on the entropy generation due to heat, it is clear from the figure that there is a strong direct proportional relationship between $Sgen_h$ and *Ra* higher than 10^4, and weak proportional relationship for *Ra* less than 10^4. The graph also shows that there is a weak inverse proportional relationship between $Sgen_h$ and *Kn*. Moreover, the graph shows a strong inverse proportional relationship between $Sgen_h$ and ϕ.

Figure 13 shows the interaction plots between parameters investigated in this work on $Sgen_h$, the graph shows that there is an interaction between *Ra* and ϕ, as they intersect. The changes that we are getting at the level of one independent variables are not changing systematically across the levels of the other independent variable. Therefore, a special effect has been achieved when combining them which comes in harmony with the opposite trends seen in Figures 8 and 9.

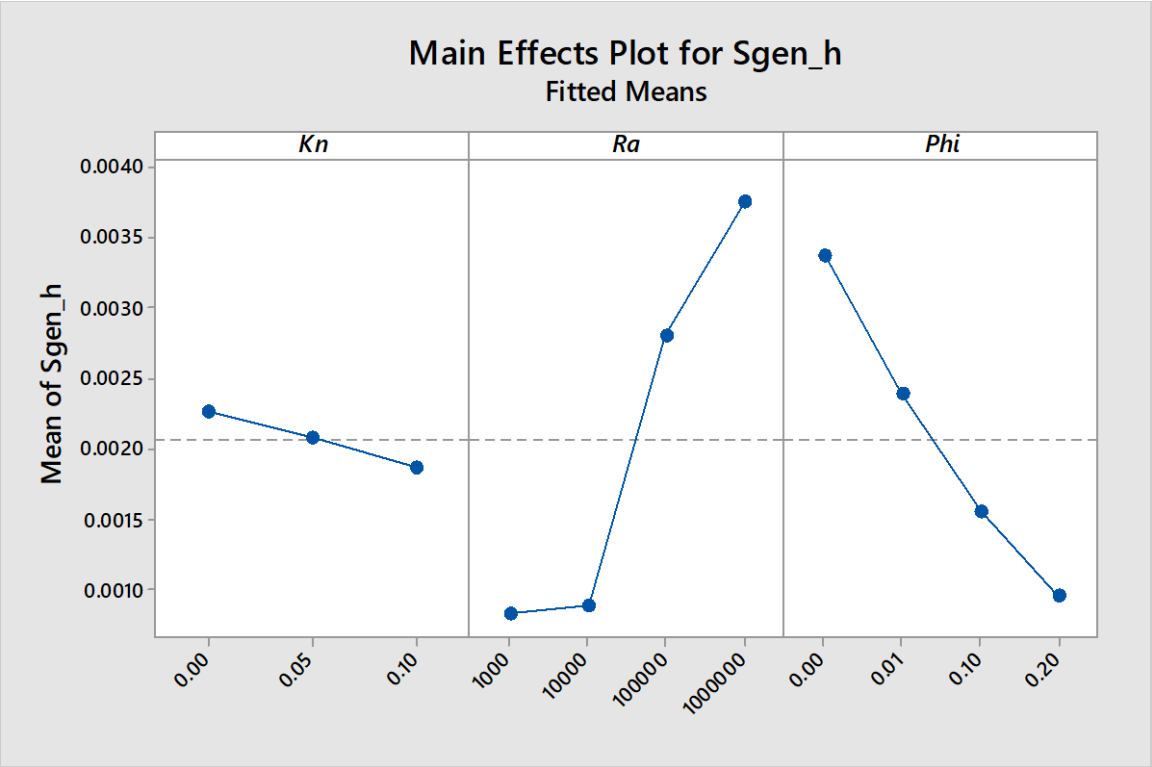

Figure 12. Main effects plot for $Sgen_h$ vs. *Kn*, *Ra* and ϕ.

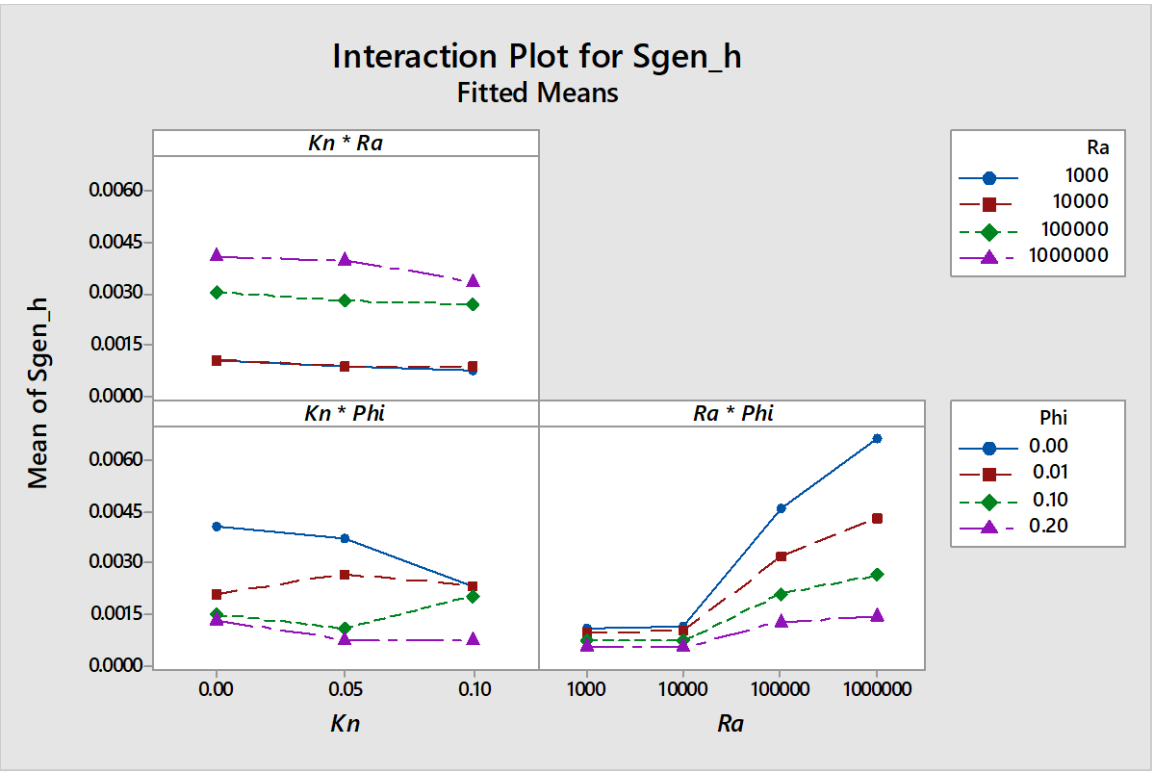

Figure 13. Interaction plot for $Sgen_h$.

Figure 14 shows the main effects of (*Kn*, *Ra* and ϕ) on the entropy generation due to flow, it is clear from the figure that there is a strong direct proportional relationship between $Sgen_f$ and *Ra*. The graph also shows that there is a strong inverse proportional relationship between $Sgen_f$ and *Kn* less than 0.05. For *Kn* greater than 0.05, there is no effect on $Sgen_f$. Moreover, the graph shows a strong

Preprints (www.preprints.org) | NOT PEER-REVIEWED | Posted: 8 January 2019 doi:10.20944/preprints201901.0074.v1

Peer-reviewed version available at Entropy 2019, 21, 103; doi:10.3390/e21020103

direct proportional relationship between $Sgen_f$ and the volume fraction of the nano solid particles for volume fractions greater than 0.01 and there is almost negligible effect for volume fractions less than 0.01.

Figure 14. Main effects plot for $Sgen_f$ vs. *Kn*, *Ra* and ϕ.

Figure 15 illustrates the interaction plots between parameters investigated in this work on $Sgen_f$, the graph shows that there is an interaction between any two parameters, as they do intersect.

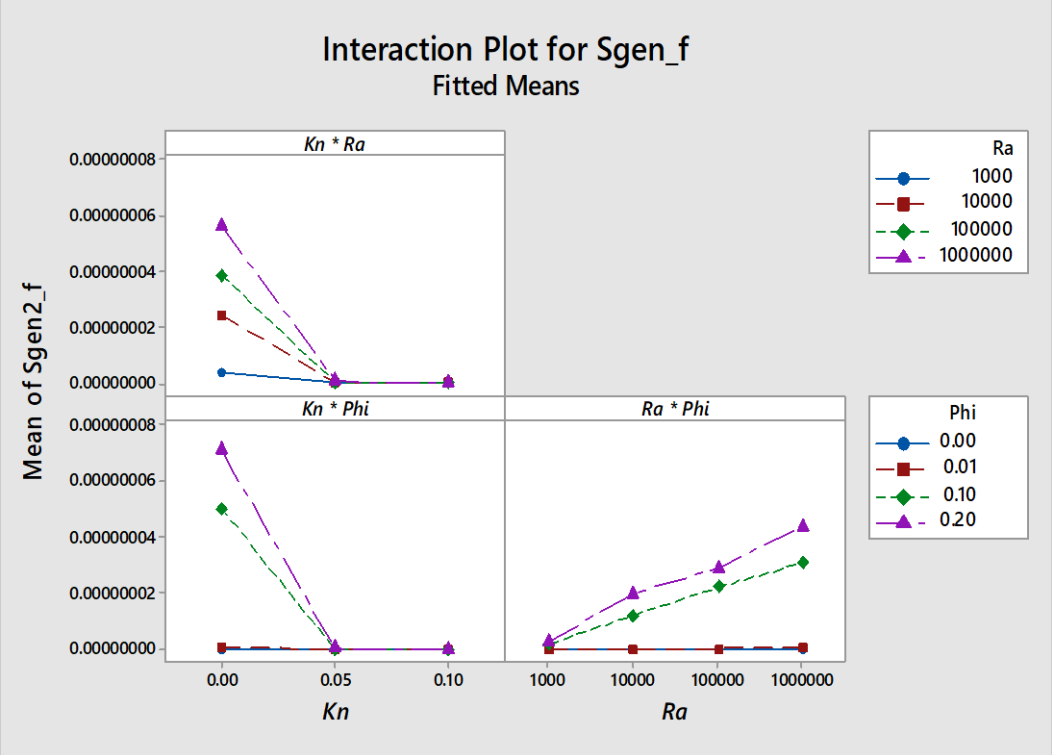

Figure 15. Interaction plot for $Sgen_f$.

Finally, in order to find the conditions at which the minimum entropy generation is obtained, optimization of the multi variable function of the total entropy generation for the parameters ranges considered in the study is conducted. The optimization that yields the minimum total entropy generation reveals that this will happen at Ra= 1001.1, ϕ= 0.19995 and Kn= 0.099 with minimum total entropy generation of 3.29e-4 kJ/kg.K

It is worth mentioning here that another simulation with the resulting conditions for the minimal entropy generation obtained from the optimization is carried out and the total entropy generation is calculated and is equal to 3.2645e-4 kJ/kg.K, which makes the optimal value extracted from the optimization of the model's correlation in a great agreement with the experimental simulation value.

4. Conclusions

Entropy generation analysis using CFD for a steady state, two-dimensional low-pressure gaseous laminar nanofluid flow inside a square cavity equipped with two solid fins attached to the hot wall is carried out. Such flows are of great importance due to their engineering applications. Rarefaction, Ra and ϕ effects on entropy generation are investigated. Results show that:

1- As Kn increases, entropy generation will decrease.
2- For low Ra numbers, the entropy generation due to flow increases as ϕ increases.
3- For higher Ra, the entropy generation due to flow decreases as ϕ increases.
4- The entropy generation due to heat increases as both Ra and ϕ increase.
5- A correlation model of the total entropy generation as a function of all the parameters investigated in this study is proposed.
6- The conditions at which the optimum (minimum) entropy generation in the investigated ranges of the parameters in this study is calculated mathematically and were validated numerically using CFD.

Author Contributions: conceptualization, Wael Al-Kouz and Ahmad Al-Muhtady; methodology, Wael Al-Kouz; software, Rama Abu-Alghanam; validation, Wahib Owhaib and Sameer Al-Dahidi; formal analysis, Wael Al-Kouz and Ahmad Al-Muhtadi; design of experiments, Ahmad Al-Muhtady; correlations, Montasir Hader; writing—original draft preparation, Wael Al-Kouz; writing—review and editing, Wael Al-Kouz and Wahib Owhaib; supervision, Wael Al-Kouz; project administration, Wael Al-Kouz.

Funding: This work is a result from partial support by German Jordanian University seed grant under Grant No. SATS 30/2016.

Conflicts of Interest: The authors declare no conflict of interest.

Nomenclature

The following notations are used in this manuscript:

Notations	
A_c	Cold wall area [m^2]
A_h	Hot wall area [m^2]
A_F	Fin area [m^2]
Be	Bejan number
C_p	Specific heat [J kg^{-1} K^{-1}]
G	Gravity acceleration in the x direction [m/s^2]
h_1	Fin 1 Position [m]
h_2	Fin 2 Position [m]
h	Convection heat transfer coefficient
K	Thermal conductivity [W m^{-1} K^{-1}]
Kn	Knudsen number

Preprints (www.preprints.org) | NOT PEER-REVIEWED | Posted: 8 January 2019 doi:10.20944/preprints201901.0074.v1

Peer-reviewed version available at Entropy 2019, 21, 103; doi:10.3390/e21020103

$\boldsymbol{k_f}$	Fluid thermal conductivity [W m^{-1} K^{-1}]
$\boldsymbol{k_{nf}}$	Nanofluid thermal conductivity [W m^{-1} K^{-1}]
$\boldsymbol{k_s}$	Nano particles thermal conductivity [W m^{-1} K^{-1}]
L	Length of the square cavity [m]
L_F	Fin length [m]
Nu	Nusselt Number
P	Pressure [Pa]
Q	Heat transfer [W]
$\boldsymbol{q_c''}$	Local heat flux at the wall of the cold surface [W/m^2]
$\boldsymbol{q_h''}$	Local heat flux at the wall of the hot surface [W/m^2]
$\boldsymbol{q_F''}$	Local heat flux at the fin [W/m^2]
R	Universal gas constant [J/mol.K]
Ra	Rayleigh number ($g\beta(T_1-T_2)L3/\alpha\nu$)
T	Temperature [°C]
T_c	Temperature of the first cell from the wall [°C]
T_i	Hot surface temperature [°C]
T_o	Cold surface temperature [°C]
T_g	Temperature of the nanofluid [°C]
T_w	Temperature of the wall [°C]
u	Velocity in x-direction [m/s]
u_c	Tangential velocity of the first cell from the wall [m/s]
u_g	Tangential velocity of the nanofluid [m/s]
u_w	Tangential velocity of the wall [m/s]
V	Velocity in y-direction [m/s]
x, y	Cartesian coordinates [m]

Greek Symbols

α	Thermal diffusivity [m^2/s]
β	Thermal expansion coefficient [1/K]
γ	Specific weight (N/m^3)
λ	Molecular mean free path (m)
μ	Dynamic viscosity [kg m^{-1} s^{-1}]
ν	Kinematic viscosity [m^2s^{-1}]
ϕ	Nano particles volume fraction %
ρ	Density of air, given by ideal gas equation (P/RT), [Kg/m^3]
σ_T	Thermal accommodation coefficient
σ_v	Momentum accommodation coefficient

Subscripts

Eff	Effective
f	Fluid
F	Fin
g	Gas flow
i	Hot wall
n	Normal
nf	Nanofluid
o	Cold wall
r	Ratio
w	Wall

References

1. Cai, J., Zhang, L., Ju, Y., Pia, G., & Zhang, Z. (2018). An Introduction to Fractal-Based Approaches In Unconventional Reservoirs — Part I. Fractals, 26(02), 1802001. doi:10.1142/s0218348x18020012
2. Shafieian, A., Khiadani, M., & Nosrati, A. (2018). A review of latest developments, progress, and applications of heat pipe solar collectors. Renewable and Sustainable Energy Reviews, 95, 273-304. doi:10.1016/j.rser.2018.07.014
3. Phiraphat, S., Prommas, R., & Puangsombut, W. (2017). Experimental study of natural convection in PV roof solar collector. International Communications in Heat and Mass Transfer, 89, 31-38. doi:10.1016/j.icheatmasstransfer.2017.09.022
4. Liang, M., Liu, Y., Xiao, B., Yang, S., Wang, Z., & Han, H. (2018). An analytical model for the transverse permeability of gas diffusion layer with electrical double layer effects in proton exchange membrane fuel cells. International Journal of Hydrogen Energy, 43(37), 17880-17888. doi:10.1016/j.ijhydene.2018.07.186
5. Long, G., Liu, S., Xu, G., Wong, S., Chen, H., & Xiao, B. (2018). A Perforation-Erosion Model for Hydraulic-Fracturing Applications. SPE Production & Operations, 33(04), 770-783. doi:10.2118/174959-pa
6. Long, G., & Xu, G. (2017). The Effects of Perforation Erosion on Practical Hydraulic-Fracturing Applications. SPE Journal, 22(02), 645-659. doi:10.2118/185173-pa
7. Mey, G. D., Torzewicz, T., Kawka, P., Czerwoniec, A., Janicki, M., & Napieralski, A. (2016). Analysis of nonlinear heat exchange phenomena in natural convection cooled electronic systems. Microelectronics Reliability, 67, 15-20. doi:10.1016/j.microrel.2016.11.003
8. Purusothaman, A. (2018). Investigation of natural convection heat transfer performance of the QFN-PCB electronic module by using nanofluid for power electronics cooling applications. Advanced Powder Technology, 29(4), 996-1004. doi:10.1016/j.apt.2018.01.018
9. Choi, S.U. S; Eastman, J.A. Enhancing thermal conductivity of fluids with nanoparticles. ASME International Mechanical Engineering Congress & Exposition **November 12-17, 1995**, San Francisco.
10. Khanafer, K.; Vafai, K.; Lightstone, M. Bouyancy driven heat transfer enhancement in a two dimensional enclosure utilizing nanofluids. *International Journal of Heat and Mass Transfer* **2003**, *46*, 3639-3653.
11. Khanafer, K.; Vafai, K. A critical synthesis of thermosphysical characteristics of nanofluids. *International Journal of Heat and Mass Transfer* **2011**, *54*, 4410-4428.
12. Boungioron, J. Convective transport in nanofluids. ASME Journal of Heat Transfer **2006,** *128*, 240-250.
13. Oztop, H.F.; Abu-Nada, E. Numerical study of natural convection in partially heated rectangular enclosures filled with nanofluids. *International Journal of Heat Fluid Flow* **2008**, *29*, 1326-1336.
14. Ghasemi, B.; Aminossadati, S.M.; Raisi, A. Magnetic field effect on natural convection in a nanofluid-filled square enclosure. *International Journal of Thermal Science* **2011**, *50*, 1748-1756.
15. Kefayati, G.H.R.; Hosseinizadeh, S.F.; Gorji, M.; Sajjadi, H. Lattice Boltzmann simulation of natural convection in tall enclosures using water/SiO_2 nanofluid. *International communication in Heat and Mass transfer* **2011**, *38*, 798-805.
16. Kefayati, G.H.R. Heat transfer and entropy generation of natural convection on non-Newtonian nanofluids in porous cavity. *Powder Technology* **2016**, *299*, 127-149.
17. Al-Kouz, W.; Alshare, A.; Kiwan, S.; Al-Muhtady, A.; Alkhalidi, A. Two-dimensional analysis of low-pressure flows in an inclined square cavity with two fins attached to the hot wall. *International Journal of Thermal Sciences* **2018**, *126*, 181-193.
18. Al-Kouz, W.; Kiwan, S.; Alkhalidi, A.; Sari, M.; Alshare, A. Numerical study of heat transfer enhancement for low-pressure flows in a square cavity with two fins attached to the hot wall using AL_2O_3-air nanofluid. *Journal of Mechanical Engineering* **2018**, *64*, 26-36.
19. Kefayati, G.H.R.; Che Sidik, N.A. Simulation of natural convection and entropy generation of non-Newtonian nanofluid in an inclined cavity using Buongiorno's mathematical model (Part II, entropy generation). *Powder Technology* **2017**, *305*, 679-703.
20. Parvin, S.; Chamkha, A.J. An analysis on free convection flow, heat transfer and entropy generation in an odd-shapped cavity filled with nanofluid. *International communications in Heat and Mass Transfer* **2014**, *54*, 8-17.
21. Mejri, I.; Mahmoudi, A.; Abbasi, M.A.; Omri, A. Magnetic field effect on entropy generation in a nanofluid-filled enclosure with sinusoidal heating on both side walls **2014,** *Powder Technology*, *266*, 340-353.

22. Mahmoudi, A.; Mejri, I.; Abbasi, M.A.; Omri, A. Analysis of the entropy generation in nanofluid-filled cavity in the presence of magnetic field and uniform heat generation/absorption. *Journal of Molecular Liquids* **2014**, *198*, 63-77.
23. Armaghani, T.; Kasaeipoor, A.; Alavi, N.; Rashidi, M.M. Numerical investigation of water-alumina nanofluid natural convection heat transfer and entropy generation in a baffled L-shaped cavity. *Journal of Molecular Liquids* **2016**, *223*, 243-251.
24. Al-Zamily, A.M.J. Analysis of natural convection and entropy generation in a cavity filled with multi-layers of porous medium and nanofluid with a heat generation. *International Journal of Heat and Mass Transfer* **2017**, *106*, 1218-1231.
25. Bouchoucha, A.E.M.; Bessaïh, R.; Oztop, H.F.; Al-Salem, K.; Bayrak, F. Natural convection and entropy generation in a nanofluid filled cavity with thick bottom wall: effect of non-isothermal heating. *International Journal of Mechanical Science* **2017**, *126*, 95-105.
26. Ashorynejad, H.R.; Hoseinpour, B. Investigation of different nanofluids effect on entropy generation on natural convection in porous cavity. *European Journal of Mechanics B/Fluids* **2017,** *62*, 86-93.
27. Sheremet, M.A.; Grosan, T.; Pop, I. Natural convection and entropy generation in a square cavity with variable temperature side walls filled with a nanofluid: Buongiorno's mathematical model. *Entropy* **2017**, *19*, *337*, 1-16.
28. Alsabery, A.I.; Ishak, M.S.; Chamkha, A.J.; Hashim, Ishak. Entropy Generation analysis and natural convection in a nanofluid-filled square cavity with a concentric solid insert and different temperature distributions. *Entropy* **2018**, *20, 336*, 1-24.
29. Siavashi, M.; Yousofvand, R.; Rezanejad, S. Nanofluid and porous fins effect on natural convection and entropy generation of flow inside a cavity. *Advanced Powder Technology* **2018**, *29*, 142-156.
30. Kashyap, D.; Dass, A.K. Two-phase lattice Boltzmann simulation of natural convection in a Cu-water nanofluid filled porous cavity: effects of thermal boundary conditions on heat transfer and entropy generation. *Advanced Powder Technology* **2018**, *29*, 2707-2724.
31. Gibanov, N.S.; Sheremet, M.A.; Oztop, H.F.; Abu-Hamdeh, N. Mixed convection with entropy generation of nanofluid in a lid-driven cavity under the effects of a heat-conducting solid wall and vertical temperature gradient. *European Journal of Mechanics / B Fluids* **2018**, *70*, 148-159.
32. Mansour, M.A.; Siddiqa, S.; Gorla, R.S.R.; Rashad, A.M. Effect of heat source and sink on entropy generation and MHD natural convection of Al_2O_3-Cu/water hybrid nanofluid filled with square porous cavity. *Thermal Science and Engineering Progress* **2018**, *6*, 57-71.
33. Rahimi, A.; Sepehr, M.; Lariche, M.J.; Kasaeipoor A.; Malekshah, E.H. Entropy generation analysis and heatline visualization of free convection in nanofluid (KKL model-based) –filled cavity including internal active fins using lattice Boltzmann method. *Computers and Mathematics with Applications* **2018**, *75*, 1814-1830.
34. Rashidi, M. M., Nasiri, M., Shadloo, M. S., & Yang, Z. (2016). Entropy Generation in a Circular Tube Heat Exchanger Using Nanofluids: Effects of Different Modeling Approaches. Heat Transfer Engineering, 38(9), 853-866. doi:10.1080/01457632.2016.1211916
35. Yarmand, H., Ahmadi, G., Gharehkhani, S., Kazi, S., Safaei, M., Alehashem, M., & Mahat, A. (2014). Entropy Generation during Turbulent Flow of Zirconia-water and Other Nanofluids in a Square Cross Section Tube with a Constant Heat Flux. Entropy, 16(11), 6116-6132. doi:10.3390/e16116116
36. Jamalabadi, M. A., Safaei, M., Alrashed, A., Nguyen, T., & Filho, E. B. (2017). Entropy Generation in Thermal Radiative Loading of Structures with Distinct Heaters. Entropy, 19(10), 506. doi:10.3390/e19100506
37. Aghaei, A., Sheikhzadeh, G. A., Goodarzi, M., Hasani, H., Damirchi, H., & Afrand, M. (2018). Effect of horizontal and vertical elliptic baffles inside an enclosure on the mixed convection of a MWCNTs-water nanofluid and its entropy generation. The European Physical Journal Plus, 133(11). doi:10.1140/epjp/i2018-12278-4
38. Mahmoudinezhad, S., Rezania, A., Yousefi, T., Shadloo, M. S., & Rosendahl, L. A. (2017). Adiabatic partition effect on natural convection heat transfer inside a square cavity: Experimental and numerical studies. Heat and Mass Transfer, 54(2), 291-304. doi:10.1007/s00231-017-2103-7
39. Nasiri, H., Jamalabadi, M. Y., Sadeghi, R., Safaei, M. R., Nguyen, T. K., & Shadloo, M. S. (2018). A smoothed particle hydrodynamics approach for numerical simulation of nano-fluid flows. Journal of Thermal Analysis and Calorimetry. doi:10.1007/s10973-018-7022-4

40. Karniadakis, G., Beskok A., Aluru, N. (2005). Microflows and Nanoflows.Springer;.
41. Lockerby, D., Reese, J., Barber, R. (2004) Velocity boundary condition at solid wall in rarefied gas calculations, Physical Review E, Vol. 70,No. 1, 017303.

42. Stéphane Colin, (2006). Heat Transfer and Fluid Flow in Minichannels and microchannels: Single-phase gas flow in microchannels, Elsevier Ltd
43. Versteeg, H., Malalasekera, W. (1995). An Introduction to Computational Fluid Dynamics: The Finite Volume Method, Prentice-Hall, Essex.
44. Patankar, S.V., Spalding, D. B., (1972). A calculation procedure for heat, mass and momentum transfer in three-dimensional parabolic flows, Int. J. of Heat and Mass Transfer 15 No. 10, 1787-1806.